This is the Pre-Published Version.

The following publication Hui Li, Yuanhong Yang, Lin Lu, and Wei Jin, "Practical reflective birefringent fiber interferometer sensor," Appl. Opt. 58, 7862-7867 (2019) is available at https://doi.org/10.1364/AO.58.007862.

Practical reflective birefringence fiber interferometer sensor

HUI LI,[1] YUANHONG YANG,[1,*] LU LIN,[1] WEI JIN[2]

[1] School of Instrumentation and Optoelectronic Engineering, Beihang University, Beijing 100191, China
[2] Department of Electrical Engineering and Photonics Research Center, The Hong Kong Polytechnic University, Hong Kong, China
*Corresponding author: yhyang@buaa.edu.cn

Received XX Month XXXX; revised XX Month, XXXX; accepted XX Month XXXX; posted XX Month XXXX (Doc. ID XXXXX); published XX Month XXXX

This paper proposes a simple and practical reflective birefringence fiber interferometer sensor scheme. Its optimized spectrum response equation was obtained and the two parameters sensor was constructed. As typical embodiment, a temperature and lateral pressure sensor with a polarization beam splitter (PBS) and two segments of solid core polarization maintaining photonic crystal fibers (PM-PCFs) was designed and investigated experimentally. Based on the advantage of ultralow temperature coefficient of PM-PCFs, a temperature insensitive lateral pressure sensor with two segments of PM-PCFs with equal length was demonstrated theoretically and experimentally. The lateral pressure sensitivity is determined to be around 0.298 nm/N. Moreover, the effect of environmental disturbance applied on PM fiber pigtail of the polarization beam splitter was investigated experimentally and proved negligible. This provides a practical temperature insensitive sensor technique for field application.

1. INTRODUCTION

Intrinsic birefringence fiber interferometer (BFI) sensors have attracted great interest due to their unique properties, such as easy manufacture, flexibility and high sensitivity [1-3]. The typical BFI schemes based on hybrid Sagnac fiber loop formed by single mode fiber directional coupler and polarization maintaining fibers (PMFs) have been studied intensively and various sensor configurations were proposed to sense pressure [4], temperature [5], torsion [6] and gas concentration [7], etc. The temperature insensitive BFIs have been demonstrated with birefringence photonic crystal fibers [8, 9] and an optical fiber reflective Lyot filter [10]. The multi-parameters sensors with high sensitivity have been achieved too by inserting long-period fiber grating or multi-segment PMFs in the Sagnac BFIs [11-13]. However, there are some drawbacks in these BFI sensors for the following reasons: First, almost all schemes use single mode fiber directional coupler and the output spectrum is hardly stable [14]. Second, the ring loop layout is inconvenient for practical implementations. Third, the polarization controller is necessary to get desired polarization states in the fiber loop. These results in large size and complex sensor structure and the Sagnac BFI sensors can only work in laboratory.

In this paper, we proposed a simple reflective BFI sensor scheme. It consists of a polarization beam splitter (PBS), two sections of birefringence fibers (BFs), and a film reflector deposited on the far end of the second BFs. We modeled the reflection spectrum response and obtained the optimized sense equation. And a two parameters sensor was constructed to measure two applied variates simultaneously and separately. Taking two segments polarization maintaining solid core photonic crystal fiber (PM-PCFs) as sense probes, we designed and investigated experimentally a temperature and lateral pressure sensor as a typical embodiment of this reflective BFI sensor scheme proposed. Furthermore, taking advantage of ultralow temperature sensitivity, we demonstrated a temperature insensitive lateral pressure sensor with two equal length PM-PCFs. Besides, we investigated experimentally the effect of the ambient temperature and lateral pressure disturbance applied on the PBS pigtail. The results proved demonstrably that the sensor is insensitive to environmental fluctuations and has great potential for field application.

2. OPERATION PRINCIPLE

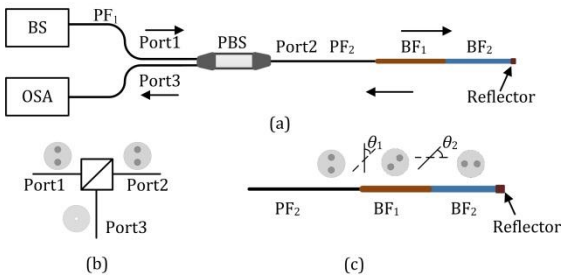

Fig. 1. Schematic illustration of (a) the reflective BFI sensor, (b) the PBS, and (c) angle offset at splicing points between BFs.

© 2019 Optica Publishing Group. One print or electronic copy may be made for personal use only. Systematic reproduction and distribution, duplication of any material in this paper for a fee or for commercial purposes, or modifications of the content of this paper are prohibited.

The schematic diagram of the reflective BFI sensor is shown in Fig. 1(a). It consists of a broadband source (BS), a commercial three ports PBS, two pieces of BFs (named as BF_1 and BF_2) and a film reflector deposited on the far end of BF_2. The schematic structure of the PBS is shown schematically in Fig. 1(b), the pigtails of Port1 and Port2 are high birefringence Panda PMFs (named as PF_1 and PF_2) and the pigtail of Port3 is single mode fiber. The PF_2, BF_1 and BF_2 are fusion spliced to each other with angle offset of θ_1, and θ_2 between their main polarization axes (as shown in Fig. 1(c)), respectively. The optical spectrum analyzer (OSA) is taken to record the reflective spectrum.

The light from the BS is polarized after traveling through the PBS from Port1 to Port2 along the fast axis of PF_2. The linearly polarized light is split at each splicing point and excited to orthogonal polarization modes along the fast and slow axis of the BFs respectively. The excited orthogonal modes are reflected at the film reflector and brought to interference when they pass through Port2 to Port3. By incorporating Jones matrix formulation and the same derivation process in [15,16], the reflection spectrum response R, as a periodic function of the wavelength, can be derived out:

$$R=(\sin 2\theta_1 \sin\varphi_1 \cos\varphi_2 + \cos 2\theta_1 \sin 2\theta_2 \sin\varphi_2 + \sin 2\theta_1 \cos 2\theta_2 \cos\varphi_1 \sin\varphi_2)^2 \quad (1)$$

$$\varphi_i = \frac{2\pi B_i l_i}{\lambda}, \quad i=1, 2 \quad (2)$$

where φ_i(i=1,2) is the phase difference induced by the ith BFs. B_i, l_i are the birefringence and length of the ith BFs respectively. λ is the operation wavelength. It can be seen that there will be one term left in Eq. (1) when θ_1 and θ_2 are both set to 45°, and Eq. (1) can be rewritten as:

$$R = (\sin\varphi_1 \cos\varphi_2)^2 \quad (3)$$

This optimized response equation indicates that the value of R will be zero when $\varphi_1=m\pi$ or/and $\varphi_2=(n+1/2)\pi$ (m, n is the integer, represents the interference order at each resonant dip) and the corresponding dip wavelength can be expressed as follows:

$$\lambda_1 = \frac{2B_1 l_1}{m} \quad (4)$$

$$\lambda_2 = \frac{2B_2 l_2}{(n+1/2)} \quad (5)$$

where λ_1 and λ_2 are the resonant dip wavelengths, $B_i l_i$ is optical path difference (OPD) between the two orthogonal modes in the ith BFs.

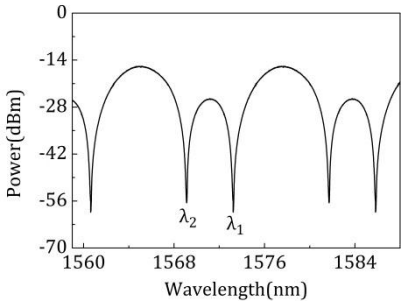

Fig. 2. Typical reflective spectrum when θ_1 and θ_2 are both set to 45°.

The typical reflective spectrum recorded by the OSA (AD6370, Yokogawa Inc.) is shown in Fig. 2. There are only two resonant dip wavelengths satisfying Eq. (4) and Eq. (5) respectively in one period and the dip wavelengths were determined independently by the OPD of BF_1 and BF_2 respectively. Moreover, the measurable range and sensitivity are mutually dependent because the spectral resolution of optical spectrum interrogator is limited and the parameters optimization is necessary to achieve desired performance for certain sensing applications.

Based on Eq. (4) and (5), a 2×2 sensing matrix can be built up for measurement of any two parameters which can modulate the OPD of the two pieces of BFs simultaneously or separately. It can be expressed as follows:

$$\begin{bmatrix}\lambda_1\\ \lambda_2\end{bmatrix} = \begin{bmatrix}A & B\\ C & D\end{bmatrix}\begin{bmatrix}x\\ y\end{bmatrix} + \begin{bmatrix}\lambda_{10}\\ \lambda_{20}\end{bmatrix} \quad (6)$$

where A, B, C, D, λ_{10} and λ_{20} are the matrix coefficients and obtained generally by experiment. In general, temperature is naturally one variate in this matrix equation as a basic parameter or crosstalk factor and another variate, such as pressure, torsion or gas concentration [8, 15, 17], is that to be measured. Furthermore, the temperature insensitive sensor may also be obtained with optimized birefringence fiber material and structure parameters. Significantly, as shown in Fig. 1(a), the effective optical interference paths in the reflective BFI sensor are all made of BFs (or PMFs) and good capability of anti-environmental interference can be guaranteed.

3. EXPERIMENT AND DISCUSSION

A. Temperature and lateral pressure sensor

Based on Fig. 1(a), a temperature and lateral pressure sensor was designed as the typical embodiment of the proposed reflective BFI sensor scheme. As shown in Fig. 3(a). It is composed of a commercial PBS (Ruik-tech Communication Co.) with extinction ratio of 35dB and two segments of solid core PM-PCFs (Yangtze Optical Electronic Co., LTD). The PM-PCFs have same birefringence of 9.05×10^{-4} and same length ~10 cm and are taken as sensing probes (BF_1 and BF_2). The film reflector is deposited on the far end of BF_2 and the reflectivity is greater than 90% at 1550 nm. An optical spectrum interrogator (SM125, Micron Optics Inc.) is taken to monitor the reflective spectrum. The Port1 of the PBS is connected to channel 2 (CH2) of SM125 and the Port3 is connected to channel 1 (CH1) via an isolator (ISO, Ruik-tech Communication Co.). The wavelength scanning range of SM125 is from 1510 nm to 1590 nm and its wavelength precision is 1 pm, this enables a large range and high-precision measurement of the reflective spectrum. The computer is taken to record the reflective spectrum and pick up the dips wavelength.

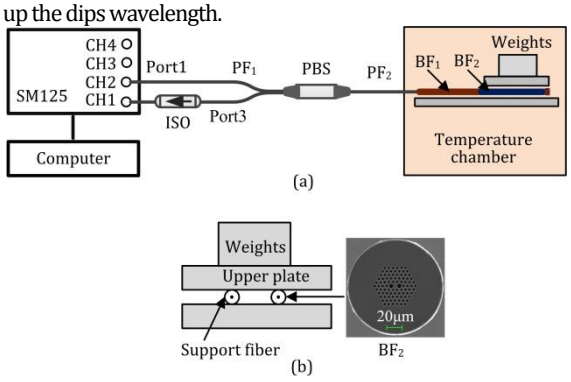

Fig. 3. Schematic of (a) the temperature and lateral pressure sensor, and (b) the lateral pressure loading setup and the direction of polarization axis of BF_2 (PM-PCF).

One of the sensing PM-PCFs, i.e. BF_2 and a same structure support fiber were sandwiched in two stainless steel plates to form a lateral

pressure experimental setup. The slow axis of BF2 was aligned to the direction of pressurization with the elasto-optic polarization measurement method described in reference [18], as shown in Fig. 3(b). The lateral pressure experimental setup with the two sensing PM-PCFs segments were mounted on a leveled stage in the temperature chamber (VT-4002, Votech Inc.) and the lateral pressure was applied by adding standard weights on the upper plate which self weight is 400 g (3.92 N). During the experimental procedure, a set of standard weights from 100 g to 2100 g with 500 g interval were added on the upper plate to apply total lateral pressure from 4.9 N to 24.5 N on BF_2. Under each lateral pressure condition, the reflective spectrums were recorded respectively when the temperature in chamber was stable at -40 °C, -20 °C, 0 °C, +20 °C, +40 °C, +60 °C. The typical spectra under 4.9 N lateral pressure and different temperature and under +20 °C temperature and different lateral pressure are shown in Fig. 4(a) and (b) respectively, where the dip wavelengths near 1573.2 nm and 1566.4 nm are selected as initial λ_1 and λ_2, respectively.

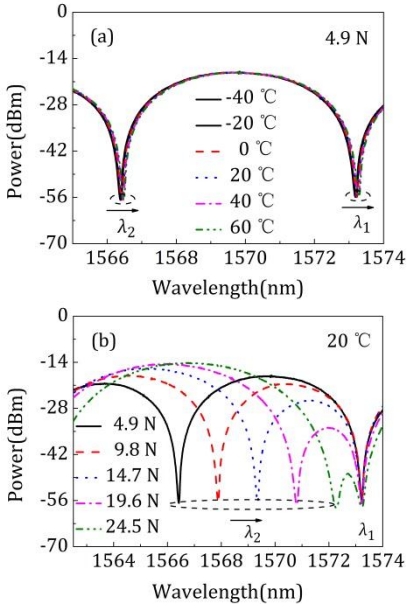

Fig. 4. Measured reflective spectra, (a) under 4.9 N and different temperature and (b) under 20 °C and different lateral pressure.

As shown in Fig. 4(a), λ_1 and λ_2 both shift slightly with temperature and they have the same temperature sensitivity because the BFs are the same PM-PCFs with equal length and the temperature coefficient of PM-PCFs is very low. In Fig. 4(b), λ_1 is stable, while λ_2 shifts longer with increasing lateral pressure. The dip wavelengths λ_1 and λ_2 under different lateral pressure and temperature within the wavelength range of 1566 nm to 1574 nm (less than one period of ~3nm) are picked up and plotted in Fig. 5(a) and (b) where lateral pressure and temperature are taken as horizontal coordinates respectively. Fig. 5(a) shows that almost all curves overlap under stable temperature and different lateral pressure. In Fig. 5(b), curves of λ_1 overlap under different temperature and lateral pressure, while curves of λ_2 are parallel to each other under different lateral pressure. These results indicate that λ_1 is unaffected by lateral pressure, but proportional to the temperature with a low coefficient, while λ_2 is proportional both to temperature and lateral pressure with a bigger pressure coefficient. Figure 5(b) also shows that λ_1 and λ_2 shift with the same temperature coefficient. Taking temperature and lateral pressure as variates of x and y in Eq. (6), the matrix coefficients under different experimental conditions were worked out and the values of average and standard deviation were listed in Table 1. The coefficients of A and C are equal to 0.0010 nm/°C when two significant digits was set. The temperatuer and lateral pressure uncertainty of this experimental measurement are about 1.0 °C and 0.01 N over the temperature and lateral ranges of 100 °C and 24.5 N respectively. The larger temperature uncertainty is due to the ultra-low temperature coefficient of PM-PCFs and the limited spectral resolution of optical spectrum interrogator.

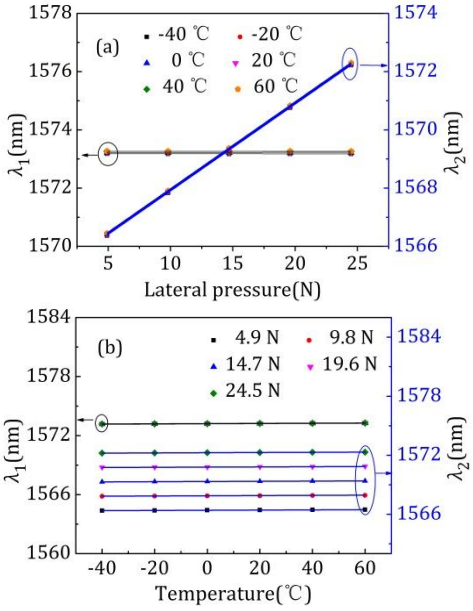

Fig. 5. (a) λ_1 and λ_2 vs. the lateral pressure under different temperature and (b) λ_1 and λ_2 vs. temperature under different lateral pressure.

As shown in Fig. 4(b), λ_1 and λ_2 may coincide if more lateral pressure is applied. This means that the measurable lateral pressure range is limited by the wavelength separation $\Delta\lambda$ between λ_1 and λ_2. From Eq. (3), (4) and (5), we can see that $\Delta\lambda$ is determined by the common factor (for example, environmental temperature) and special factor (for example, the lateral pressure) to be measured, and there must be a special optimized operating condition for certain sensing application and this condition can be achieved by selecting suitable PMFs probes with desired sensitivity and optimized length. For the sensor with PM-PCFs probes shown in Fig. 3(a), only the measurable range of lateral pressure need be optimized independently because the shift of λ_1 and λ_2 due to temperature is quite small. And $\Delta\lambda$ can be enlarged by shortening the length of BF_1 and lengthening the length of BF_2 in one period, but the longer BF_2 will result in higher sensitivity and compress the measurable range in reverse and careful optimization is needed.

According to the above disscusion, the length of BF_1 and BF_2 were changed to 7cm and 12cm respectively in the sensor shown in Fig. 3(a) and the initial $\Delta\lambda$ was increased from ~6.8 nm to ~7.2 nm. The same experimental process was repeated and the sensing performance was investigated for this case of unequal length PM-PCFs. The two parameters, i.e. temperature and lateral pressure, were measured simultaneously and the temperature coefficient of BF_1 was decreased while the lateral pressure coefficient was increased. And the measurable maximum lateral pressure was extended to ~ 29.4 N. The corresponding average value and standard deviation of matrix coefficients of Eq. (6) were worked out and listed in Table 2. The shorter length of BF_1 makes the coefficient A lower than the situation that l_1=l_2=10cm, while the longer length of BF_2 results in bigger lateral pressure coefficients D. And the measurable pressure range was extended effectively. The experimental investigation results agree well with the above prediction.

Table 1. Average Value and Standard Deviation of Model Parameters when l_1=l_2=10cm

	A (nm/°C)	B (nm/N)	C (nm/°C)	D (nm/N)	λ_{10} (nm)	λ_{20} (nm)
Average value	0.0010	0	0.0010	0.298	1573.209	1564.942
Standard deviation	4.09×10^{-6}	0	1.65×10^{-6}	6.05×10^{-5}	2.69×10^{-4}	4.66×10^{-4}

Table 2. Average Value and Standard Deviation of Model Parameters when l_1=7cm, l_2=12cm

	A (nm/°C)	B (nm/N)	C (nm/°C)	D (nm/N)	λ_{10} (nm)	λ_{20} (nm)
Average value	0.00047	0	0.0011	0.324	1574.284	1565.556
Standard deviation	3.16×10^{-6}	0	2.36×10^{-6}	6.47×10^{-5}	2.18×10^{-4}	4.39×10^{-4}

B. Temperature insensitive lateral pressure sensor

As shown in Fig. 5 and Table 1, the shifts of λ_1 and λ_2 induced by temperature are almost the same and their temperature coefficient A and C are equal too. This result is attributed to the ultralow birefringence temperature coefficient (~10^{-9} /°C) of PM-PCFs [19] and the equal length of BF_1 and BF_2. The experimental results imply that temperature insensitive lateral pressure may be obtained with equal length PM-PCFs sensor probes.

Assuming the lengths of BF_1 and BF_2 are l_1 and l_2 respectively, the intrinsic birefringence of PM-PCFs is B_0, the excess birefringence induced by lateral pressure and temperature is B_P and B_T respectively, and the integer m, n in Eq(4) and (5) are equal. we can derive out the wavelength difference $\Delta\lambda$ between λ_1 and λ_2 as following:

$$\Delta\lambda = \lambda_1 - \lambda_2 = \frac{2\mathrm{m}\left(B_0 + B_T\right)\left(l_1 - l_2\right)}{m\left(m+1/2\right)} + \frac{B_0 l_1 + B_T l_1 - 2\mathrm{m}B_P l_2}{m\left(m+1/2\right)} \quad (7)$$

When the length of BF_1 and BF_2 is equal, the first term and the temperature crosstalk term can be ignored due to ultra-low birefringence temperature coefficient B_T of PM-PCFs. Eq. (9) can be rewritten as follows:

$$\Delta\lambda = \lambda_1 - \lambda_2 = l_1\left(\frac{B_0}{m(m+1/2)} - \frac{2B_P}{(m+1/2)}\right) \quad (8)$$

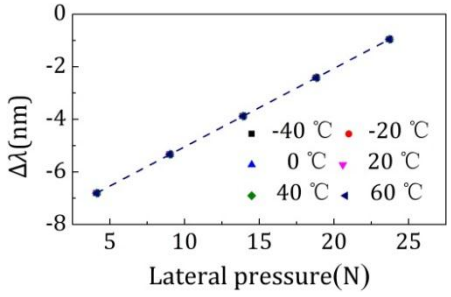

Fig. 6. Curves of $\Delta\lambda$ vs. lateral pressure under different temperature.

We can see that $\Delta\lambda$ will be temperature insensitive and proportional to B_P induced by lateral pressure. Using the experimental data obtained in the case of equal length PM-PCFs, we calculated out $\Delta\lambda$ under different lateral pressure and temperature. The curves of $\Delta\lambda$ vs. lateral pressure is plotted in Fig. 6. These curves under different temperature are almost overlapped and the lateral pressure sensitivity is around 0.298 nm/N, which is the same as the result obtained by the 2×2 sensing matrix in Eq. (6). This proves this lateral pressure is temperature insensitive by taking equal length PM-PCFs as sensing probes.

C. Effect of environmental disturbance

As shown in Fig. 3(a), the PBS pigtail PF_2 is the main part that can be affected by environmental disturbance and bring excess error to the sensor unit. To investigate the error induced by environmental disturbance, the experimental setup was designed and is shown in Fig. 7, both BF_1 and BF_2 were inserted in a glass tube immersed in the oil bath (1025A, Xiangan TestEquipment FTY) and kept stable at 25°C. The most of pigtail PF_2 was sandwiched in the lateral pressure experimental setup with arbitrary polarization axis direction and mounted in the temperature chamber. A set of standard weights from 100 g to 1100 g with 500 g interval were added on upper plate to apply lateral pressure 4.9 N to 14.7 N to simulate random lateral pressure disturbance on PF_2 and the temperature in chamber was set from -40 °C to 60 °C with interval of 25 °C to simulate random environmental temperature. The drift of λ_1 and λ_2 under different temperature and lateral pressure were picked up and displayed in Fig. 8, which are very small and random. The standard deviations of λ_1 and λ_2 are 0.0003 nm and 0.0002 nm. The equivalent temperature and lateral pressure error are ~0.3 °C and ~ 0.0001 N respectively. The errors due to environmental disturbance applied on PF_2 are far less than the uncertainty of measurement above and can be ignored. The experimental investigation proves this sensing unit insensitive to environmental fluctuations.

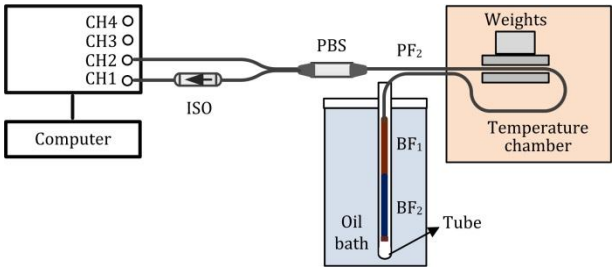

Fig. 7. Experimental setup for investigation on error induced by environmental disturbance.

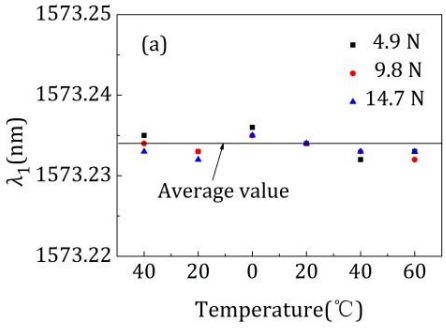

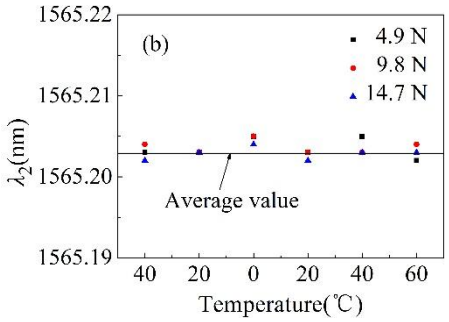

Fig. 8. Drift of (a) λ_1 and (b) λ_2 when different temperature and lateral pressure were applied on PF_2.

4. SUMMARY

A practical and simple reflective BFI sensor with the capability of two parameters sensing has been proposed and demonstrated theoretically and experimentally. The whole optical interference paths of the proposed sensor was made of PMFs and this makes the sensor practical. As a typical embodiment, a temperature and lateral pressure sensor with two segments of solid core PM-PCFs was designed and investigated experimentally and the low temperature sensitivity of 0.0010 nm/°C and high lateral pressure sensitivity of 0.298 nm/N were achieved simultaneously. Based on theoretical analysis and experimental investigation, a temperature insensitive lateral pressure sensor with two equal lengths PM-PCFs was realized and the lateral pressure sensitivity of around 0.298 nm/N was obtained. Furthermore, the effect of environmental temperature and lateral pressure disturbance applied on PBS PMF pigtails were investigated experimentally and proved negligible. This proved the proposed sensor is insensitive to environmental disturbances. It has great potential applications in the field of physics, biology and chemistry, etc.

Funding Information. National Natural Science Foundation of China (U1637106, 61227902); National Key R&D Program of China (2018YFC1503703); Program for Innovative Research Team in University (IRT 1203).

References

1. B. H. Kim, S. H. Lee, A. Lin, C. Lee, J. Lee, and W. Han, "Large temperature sensitivity of Sagnac loop interferometer based on the birefringent holey fiber filled with metal indium," Opt. Express **17**, 1789-1794 (2009).
2. E. Reyes-Vera, C. M. B. Cordeiro, and P. Torres, "Highly sensitive temperature sensor using a Sagnac loop interferometer based on a side-hole photonic crystal fiber filled with metal," Appl. Opt. **56**, 156-162 (2017).
3. H. Y. Fu, H. Y. Tam, L. Y. Shao, X. Dong, P. K. A. Wai, C. Lu, and S. K. Khijwania, "Presure sensor realized with polarization-maintaining photonic crystal fiber-based Sagnac interferometer," Appl. Opt. **47**, 2835-2839 (2008).
4. N. Ayyanar, D. Vigneswaran, M. Sharma, M. Sumathi, M. M. S. Rajan, and S. Konar, "Hydrostatic pressure sensor using high birefringence photonic crystal fibers," IEEE Sens. J. **17**, 650-656 (2017).
5. J. Shi, Y. Wang, D. Xu, H. Zhang, G. Su, L. Duan, C. Yan, D. Yan, S. Fu, and J. Yao, "Temperature Sensor Based on Fiber Ring Laser With Sagnac Loop," IEEE Photonics Technol. Lett. **28**, 1 (2016).
6. W. Chen, S. Lou, L. Wang, H. Zou, W. Lu, and S. Jian, "Highly sensitive torsion sensor based on Sagnac interferometer using side-leakage photonic crystal fiber," IEEE Photonics Technol. Lett. **23**, 1639-1641 (2011).
7. Y. Yang, F. Yang, H. Wang, W. Yang, and W. Jin, "Temperature-insensitive Hydrogen Sensor with Polarization-Maintaining Photonic Crystal Fiber-Based Sagnac Interferometer," J. Lightwave Technol. **28**, 1011-1015 (2014).
8. B. Xu, C. L. Zhao, F. Yang, H. Gong, D.N. Wang, J. Dai, and M. Yang, "Sagnac interferometer hydrogen sensor based on panda fiber with Pt-loaded WO3/SiO2 coating," Opt. Lett. **41**, 1594-1597 (2016).
9. D. H. Kim, and J. U. Kang, "Sagnac loop interferometer based on polarization maintaining photonic crystal fiber with reduced temperature sensitivity," Opt. Express **12**, 4490-4495 (2004).
10. B. Huang, Y. Wang, C. Mao, and Y. Wang, "Temperature-and strain-insensitive transverse load sensing based on optical fiber reflective Lyot filter," Appl. Phys. Express **12**, 076501 (2019).
11. O. Frazão, L. M. Marques, S. Santos, J. M. Baptista, and J. L. Santos, "Simultaneous measurement for strain and temperature based on a long-period grating combined with a high-birefringence fiber loop mirror," Photonics Technol. Lett. **18**, 2407-2409 (2006).
12. G. Sun, D. S. Moon, and Y. Chung, "Simultaneous temperature and strain measurement using two types of high-birefringence fibers in Sagnac loop mirror," Photonics Technol. Lett. **19**, 2027-2029 (2007).
13. J. Kang, X. Dong, C. Zhao, W. Qian, and M. Li, "Simultaneous measurement of strain and temperature with a long-period fiber grating inscribed Sagnac interferometer," Opt. Commun. **284**, 2145-2148 (2011).
14. D. Leandro, M. Bravo, M. Lopez-Amo. "High resolution polarization-independent high-birefringence fiber loop mirror sensor," Opt. Express **23**, 30985-30990 (2015).
15. K., Sasaki, M. Takahashi, and Y. Hirata, "Temperature-insensitive Sagnac-type optical current transformer," J. Lightwave Technol. **33**, 2463-2467 (2015).
16. Y. Liu, B. Liu, X. Feng, W. Zhang, G. Zhou, S. Yuan, G. Kai, and X. Dong, "High-birefringence fiber loop mirrors and their applications as sensors," Appl. Opt., **44**, 2382-2390 (2005).
17. Y. Yang, L. Lu, F. Yang, Y. Chen, and W. Jin, "The fiber optic Sagnac interferometer and its sensing application," OGC, **1,** 1-6 (2015).
18. Y. Yang, L. Lu, S. Liu, W. Jin, Z. Han, and Y. Cao, "Temperature-insensitive pressure or strain sensing technology with fiber optic hybrid Sagnac interferometer," Proc. SPIE. **9852**, 985216 (2016).
19. Y. Yang, J. Li, W. Duan, X. Zhang, W. Jin, and M. Yang, "An embedded pressure sensor based on polarization maintaining photonic crystal fiber," Meas. Sci. Technol. **24**, 094004 (2013).